Implementation Method in Blind Deconvolution Based Tumor Segmentation Using Simulated PET Images

Alpaslan KOÇ[1], Albert GÜVENİŞ[1]
[1]Biyomedikal Mühendisliği Enstitüsü, Boğaziçi Üniversitesi, İstanbul, Türkiye
{ alpaslan.koc, guvenis}@boun.edu.tr

***Abstract*— PET imaging is increasingly used in determining functional tumor volumes for therapy response assessment and treatment planning. Accurate measurement of metabolically active tumors may improve optimal delivery of radiation treatment. However, volume measurement of small tumors (<2 cm) has been a much investigated subject due to Partial Volume Effect and limited resolution of the system. This research combined two methods in improving accuracy of small tumor volume estimation: the tumor targeted blind deconvolution and the resampling method, and assessed it using the thresholding method on simulated PET images of tumors sized 10.5 mm and 14 mm at Tumor to Background Ratios (TBRs) of 4:1 and 10:1 reconstructed with (AW)-OSEM algorithm. Results showed that the local blind deconvolution method significantly decreased volume error rate of small tumors (<2 cm) compared with the original non-deconvolved images. The segmented mean volumes and SDs were 7.13 cc ± 2.64 cc and 1.54 cc ± 0.51 cc for the tumors in original images and locally deconvolved images respectively. The best segmented volume was measured in locally deconvolved and resampled image for the tumor size of 14 mm at TBR of 10. The estimated volume error rate was found as 0.74% for this tumor. In addition, the computation time is significantly reduced ~ 13-fold using the local extraction method with resampling. Unlike previous studies, we combined two methods and optimized iterations of deconvolution to enhance resolution of small tumor images. Our results may facilitate improvements in detection of small tumors with different shapes and heterogenous activity distributions.**

Keywords — image enhancement; image segmentation; Positron Emission Tomography; radiotherapy planning; small tumors.

I. INTRODUCTION

PET Imaging is increasingly used in Radiation Treatment Planning (RTP) to identify metabolic tumor volume [1]. Accurate estimation of tumor volume is important to prevent damage to the healthy tissues and misuse of radiation on tumor tissues. However, the volume measurement of small tumors (< 2 cm) in nuclear medicine is suffered due to the Partial Volume Effect (PVE). If the tumor size is less than 3 times the spatial resolution of the PET imaging system (~5 mm), the tumor is seen larger than real size within reconstructed image. This blurring effect stems from the result of the convolution of the real object and the system Point Spread Function (PSF) as well as image sampling procedure [2]. Soret et al. [2], Bettinardi et al. [3], and Erlandsson et al. [4] explained the practical consequences of the PVE and the partial volume correction (PVC) methods. All correction methods are applied either during or post reconstruction processes using recovery coefficient method (RC), geometric transfer matrix correction method (GTM), and the recovery of the spatial resolution of the imaging system. Image reconstruction, deconvolution, multi resolution approach, and anatomical imaging techniques facilitate the recovery of the spatial resolution of the system. Unlike these correction methods, Guvenis et al. [5] focused on the recovery of the resolution of the reconstructed PET phantom images without a known PSF information of the imaging system, i.e. they implemented the blind deconvolution on PET images during post-reconstruction process.

The segmentation processes in 3 dimensions (3-D) have been widely used in nuclear medicine imaging to accurately determine tumor volume. Segmentation of PET images may be grouped into several categories: manual segmentation, thresholding based methods, stochastic and learning based methods, region based segmentation methods, boundary based methods, and joint segmentation methods. These methods have been implemented for either physical phantom or simulation data with ground truth or clinical data, and their performances have been evaluated using various figures of merit: relative volume error, similarity index, distance measurement, and shape characterization [6]. Foster at al. [6] reviewed the literature and compared the segmentation results of PET images. Studies on the literature have generally focused on the derivation of the new segmentation methods and/or improvement of the existing methods. However, accurately measurement of the small tumors remains a major challenge.

This study aims to accurately estimate the small tumor volumes using the best parameters of the local blind deconvolution with resampling, and thus to minimize partial volume error in tumor size. The PSF is spatially-variant in PET images. We compensate for spatially-

978-1-5386-0633-9/17/$31.00 ©2017 IEEE

variant resolution by local extraction method. In addition, this method can be used as post processing necessitating widely available tools.

II. MATERIALS AND METHODS

A. Data

The data used in the study was the realistic 3-D whole body 18F-FDG PET oncology images from the OncoPET_DB database [7], [8]. A patient was modeled based on the Zubal phantom with activity concentrations obtained from a series of 70 clinical cases. The spheres resembling tumors of real lymphoma patients, with diameters of 10.5 mm and 14 mm at two different TBR of 4:1 and 10:1, have been incorporated inside the real patient volumes [Fig. 1]. The realistic PET images were simulated using the PET-SORTEO Monte Carlo simulation platform that has been validated for the geometry of the ECAT EXACT HR+ scanner operating in 3-D acquisition mode and then reconstructed with fully attenuation-weighted (AW)-OSEM algorithm with six iterations, 16 subsets, and a Gaussian isotropic post-filtering of 8 mm. The matrix size was 128 x 128 x 375 voxels for each image with a voxel size of 5.0625 mm x 5.0625 mm x 2.425 mm.

B. Cropping

This study has been divided into the two parts: The first part deals with the segmentation of the tumors on the original images obtained from the data. In the second part, the local blind deconvolution with resampling has been implemented on the locally extracted regions and tumor volumes have been evaluated.

C. Resampling

The simulated PET oncology images had a voxel resolution of 5.0625 mm, 5.0625 mm, and 2.425 mm in 3-D space. The z dimension of voxels was smaller than the x and y dimensions, thereby yielding non-cubic voxels in images. These anisotropic voxels were interpolated to isotropic pixel resolution in 1 mm. We used the trilinear interpolation method to resample PET images due the noisy characterization of PET image voxels [9].

Recently, researchers have shown an increased interest in using nuclear medicine imaging modalities with CT and MRI, i.e. high resolution anatomical images. These high quality anatomical images have smaller voxel sizes than PET and SPECT images. In order to achieve accurate registration between functional and anatomical images, PET or SPECT images with a larger voxel volume have been interpolated to smaller voxels [10]. Therefore, the first reason for choosing 1 mm isotropic pixel resolution for PET images is that the real shape and activity distribution of the interested objects in interpolated images can be recovered accurately. Hence, we can avoid inaccurate PVC errors, alignment of pixels, and segmentation before coregistration of functional and anatomical images. Another advantage of using resampling is on the usage of the assumed PSF kernels during

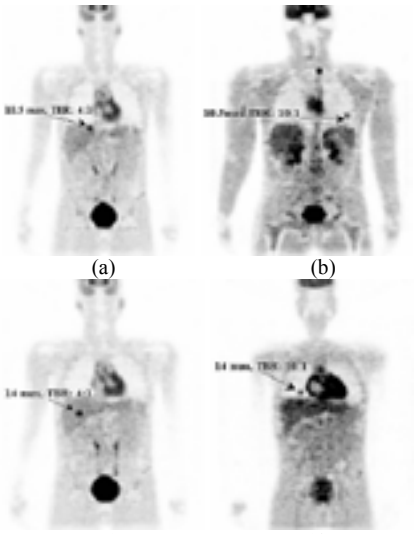

(a) (b) (c) (d)

Fig. 1. The coronal slices of 3-D whole-body 18F-FDG PET images having diameters of 10.5 mm at TBR of 4:1 (a), 10.5 mm at TBR of 10:1 (b), 14 mm at TBR of 4:1 (c), and 14 mm at TBR of 10:1.

FWHM (mm)	FWTM (mm)	Approximated PSF Size (mm)
5	12.8	13x13x13
6	15.3	15x15x15
7	17.9	17x17x17
8	20.4	21x21x21

Table 1. PSF estimation

implementation of the blind deconvolution algorithm. We can use only 3 or 4 voxels on image grid for PSF kernels without resampling. However, interpolation provides great benefit on implementation of the assumed PSF kernels on image domain considering the change of PET spatial resolution of 5 to 8 mm i.e. the PSF kernels of 13, 15, 17, and 21 voxels are used for the spatial resolutions of 5, 6, 7, and 8 mm respectively [Table 1].

D. Blind Deconvolution

Blind Image Deconvolution is a technique that recovers the true image from the observed image with no information about the true image and the blurring factor of the imaging system. The observed image (g) is mathematically expressed by

$$g = H * f + n\,. \qquad (1)$$

The deconvolution has been performed using the MATLAB (deconvblind) function [11]. It estimates the original true image using input parameters, i.e. the blurred 3D image (f) and the estimated PSF (H). Estimation is carried out for only PSF size and it is used to obtain the true PSF function for each iteration. The two parameters, the initial estimate for the PSF size and the number of iterations, could affect the recovery of the true image from the observed blurred image. The algorithm determines the true image and the PSF in given optimum initial PSF size and the number of iterations.

E. Stopping Criterion for the PSF Size and the Iteration

In an attempt to determine the stopping criterion of the iteration number and PSF size, we used the contrast to noise ratio for original and deconvolved images. The CNR is mathematically expressed by

$$\mathrm{CNR} = \frac{\bar{\mathrm{I}}_{tumor} - \bar{\mathrm{I}}_{background}}{\mathrm{SD}_{background}} . \quad (2)$$

$\bar{\mathrm{I}}_{tumor}$ displays the mean intensity of tumor voxels, $\bar{\mathrm{I}}_{background}$ displays the mean intensity of background voxels outside the tumor and $\mathrm{SD}_{background}$ displays the standard deviation of the voxel intensities within the background regions [12]. Before CNR calculations, tumors and background regions are determined with threshold intensity using the level set VOI technique on central slice of the images [Fig. 2].

Spatial resolution (FWHM) of the PET imaging system varies between 5 and 8 mm. We assume iso-gaussian PSF with FWTM. The FWTM is approximately equals 3σ for the left and 3σ for the right size. The total FWTM size of the PSF equals to the 6σ for both x, y, and z direction. The relationship between the FWHM and the σ is: FWHM = 2.35 x σ. Therefore, the tail size of the PSF = $\frac{FWHM}{2.35}\ x\ 6$ [Table 1]. The best PSF size is determined from these approximated PSF sizes considering the best CNR value for the deconvolved image at 1 iteration.

F. Segmentation

The fixed thresholding method (50% of maximum intensity value) was used to estimate the volumes of the tumors: The MIPAV software was used for implementation of the tumor segmentation algorithm [13], [14]. The following equation (3) shows calculation of the fix thresholding method after the deconvolution processes.

$$Threshold = (\bar{\mathrm{I}}_{tumor} - \bar{\mathrm{I}}_{background})\ x\ 50\% + \bar{\mathrm{I}}_{background} \quad (3)$$

G. Error Evaluation

Various figures of merit can evaluate the results of delineation method from phantoms, simulations, and patient data. The simplest measurement is comparing the volume of delineated lesions with their true values, which is measured by the volume detection error (DEvol) [6]. The volume detection error was determined as in (4).

$$DE_{vol} = \frac{(V_{det} - V_{true})}{V_{true}} \times 100\% \quad (4)$$

In (4), V_{det} was the estimated volume and V_{true} was the true spherical volume.

III. RESULTS

A. The PSF Size and the Iteration Number

Initially, the tumor and the background regions are selected using the level set VOI method after resampling process before blind deconvolution. Then CNR values were calculated for all approximated PSF sizes for each tumor at 1 iteration. The maximum CNR value enables us to determine the best PSF size for our implementation. In the next step, we have determined the best iteration number for the given best PSF size with the maximum CNR value. Table 2. indicates the optimum PSF size and the iteration number for each tumor.

Fig. 2. Tumors and background regions are determined with threshold intensity using the level set VOI technique on central slice of the cropped images.

The Tumors	The Best PSF Size(mm)	The Best Iteration Number
14 mm, 10 TBR	17x17x17	15
14 mm, 4 TBR	15x15x15	15
10.5 mm, 10 TBR	17x17x17	15
10.5 mm, 4 TBR	15x15x15	20

Table 2. Calculated PSF sizes and iteration numbers

B. The CNR Comparison

The following table shows the results for the obtained CNR values of the images before and after the deconvolution process. It is clearly indicating that the CNR values increase with the best PSF size and the iteration number after deconvolution. In the next step, we have put the recovered tumor image into the segmentation process.

The Tumors	CNR	
	Original	**Deconvolved**
14 mm, 10 TBR	9.49	21.92
14 mm, 4 TBR	5.69	11.74
10.5 mm, 10 TBR	4.75	15.27
10.5 mm, 4 TBR	4.43	13.03

Table 3. The CNR values for each tumor before and after deconvolution.

C. The Volume Measurement Results

The segmented mean volumes and SDs are 7.13 cc ± 2.64 cc and 1.54 cc ± 0.51 cc for the tumors in original images and locally deconvolved images respectively. The ground truth mean volume is 1.08 cc ± 0.51 cc. The best measured volume value is 1.54 cc for the tumor size of 14 mm at TBR of 10. When the TBR value decreases, the estimated percentage error rate increases. For instance, the volume measurement error percentages increase from 0.74% to 57.01% and from 58.42% to 85.94% for the tumor sizes of 14 mm and 10.5 mm respectively.

D. The Time Cost Analysis

Another advantage of the local extraction method with resampling is that the computation time decreases with local blind deconvolution compared with whole image deconvolution. The CPU time is calculated considering the best iteration number obtained from Table 2. The iterative

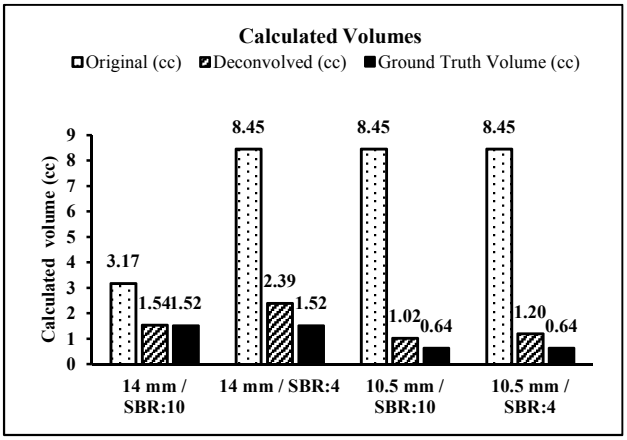

Fig. 3. Calculated volumes of the simulated images.

Tumor Regions	The Best Iteration Number	CPU Time of the whole image deconvolution (sec)	CPU Time of the local blind deconvolution (sec)
14 mm, 10 TBR	15	89.2	8
14 mm, 4 TBR	15	89.6	6.6
10.5 mm, 10 TBR	15	89.6	6.4
10.5 mm, 4 TBR	20	101.5	6.5

Table 4. The comparison of the execution times of the local blind deconvolution and the whole image blind deconvolution.

process of the local blind deconvolution algorithm is terminated after 15 or 20 iterations before a decrease of the CNR value. The initial assumed spatially-invariant PSF kernel of the blind deconvolution algorithm is 4x4x4 voxels for whole original image region. Execution time comparisons of these two distinct implementation methods are given in Table 4. The algorithms are implemented using MATLAB® 2015a on a dual core 2.53 GHz Intel® Core i5 CPU. The computation time is significantly reduced ~ 13-fold using the local extraction method.

IV. DISCUSSIONS AND CONCLUSIONS

In this study, we combined two techniques, the local blind deconvolution method and resampling, to improve the accuracy of small tumor volume estimation on PET simulated images. It was found that our proposed method to deconvolve simulated images with small tumors, i.e. < 20 mm, decreased the volume error rate to 0.74% compared with non-deconvolved images. The results showed that implementing this method only on target regions locally with optimum iteration number and approximated PSF size increased voxel intensities of target regions to higher levels while decreasing those of background voxels to lower levels [Fig. 3]. Thus, blurring effects observed on target regions resulting from the convolution of the real object and the PSF of the system can be compensated for.

Further investigation and experimentation on segmentations of the small tumors is strongly recommended to accurately determine the biological target volume. It would be interesting to assess the effects of other tumor shapes and heterogeneous activity distributions on the accurate estimation of the tumor volumes using this experimental set up with other segmentation methods for the radiotherapy planning.

REFERENCES

[1] Tinsu Pan, Osama Mawlawi, "PET/CT in radiation oncology," Med. Phys., vol. 35, no. 11, pp. 4955-4966, 2008.

[2] M. Soret, Stephen L. Bacharach, I. Buvat, "Partial-Volume Effect in PET Tumor Imaging," J. Nucl. Med., vol. 48, no. 6, pp. 932-945, June 2007.

[3] V. Bettinardi, I. Castiglioni, E. De Bernardi, M. C. Gilardi, "PET quantification: strategies for partial volume correction," Clin. Transl. Imaging, vol. 2, pp. 199-218, July 2014.

[4] K. Erlandsson, I. Buvat, P. H. Pretorius, B. A. Thomas, B. F. Hutton, "A review of partial volume correction techniques for emission tomography and their applications in neurology, cardiology and oncology," Phys. Med. Biol., vol. 57, pp. R119–R159, Oct. 2012.

[5] A. Guvenis, A. Koc, "Optimising delineation accuracy of tumours in PET for radiotherapy planning using blind deconvolution," Radiat. Prot. Dosimetry, Vol. 165, No. 1–4, pp. 495–498, Jul. 2015.

[6] B. Foster, U. Bagci, A. Mansoor, Z. Xu, D. J. Mollura, "A review on segmentation of positron emission tomography images," Computers in Biology and Medicine, vol. 50, pp. 74–96, 2014.

[7] S. Tomei, A. Reilhac, D. Visvikis, N. Boussion, C. Odet, F. Giammarile, and C. Lartizien, "OncoPET_DB: A Freely Distributed Database of Realistic Simulated Whole Body 18F-FDG PET Images for Oncology," IEEE Transactions on Nuclear Science, vol. 57, pp. 246-255, Feb. 2010.

[8] Creatis.insa-lyon.fr. (2017). Softwares-Releases | CREATIS. [online] Available at: https://www.creatis.insa-lyon.fr/oncoPET_DB/ [Accessed 18 May. 2015].

[9] Erlandsson, Kjell. "Partial Volume Correction in PET Imaging." Basic Science of PET Imaging. Springer International Publishing, 2017. 355-378.

[10] Hoetjes, Nikie J., et al. "Partial volume correction strategies for quantitative FDG PET in oncology." European journal of nuclear medicine and molecular imaging 37.9 (2010): 1679-1687.

[11] Mathworks.com. (2017). Deblur image using blind deconvolution - MATLAB deconvblind - MathWorks United Kingdom. [online] Available at: https://www.mathworks.com/help/images/ref/deconvblind.html

[12] Smith, Nadine Barrie, and Andrew Webb. Introduction to medical imaging: physics, engineering and clinical applications. Cambridge university press, 2010.

[13] M. J. McAuliffe, F. M. Lalonde, D. McGarry, W. Gandler, K. Csaky, B. L. Trus, "Medical Image Processing, Analysis and Visualization in clinical research," IEEE COMPUTER-BASED MEDICAL SYSTEMS (CBMS) 2001, 381-386.

[14] The National Institutes of Health Center for Information Technology (CIT), MIPAV, version 7.3.0 (computer software), Rockville, Maryland, 2015